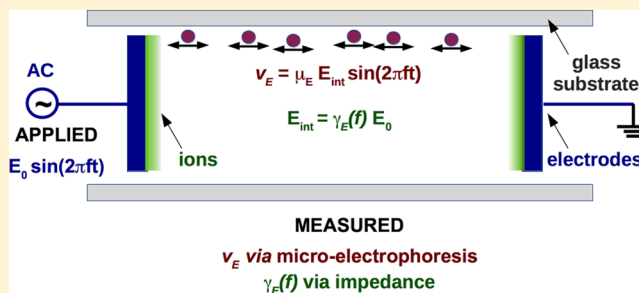


Frequency-Dependent Solvent Impedance and Colloid Microelectrophoresis Measurements in Partially Polar Solvents

Edward Hayden, Zena Aljabal, and Anand Yethiraj*[✉]

Department of Physics and Physical Oceanography, Memorial University, St. John's, Newfoundland A1B 3X7, Canada

ABSTRACT: We carry out frequency-dependent solvent impedance measurements and alternating current (ac) colloid microelectrophoresis experiments in partially polar solvents in the low-frequency regime ($0.25 \text{ Hz} \leq f \leq 10 \text{ Hz}$). Solvent electrode polarization effects are quantified first in partially polar solvent mixtures containing bromocyclohexane (CHB). We find that the polarization capacitance from electrode polarization exhibits a clear power law behavior $C_p = C_{p0} f^{-m}$ with power law exponent $m = 0.25 \pm 0.04$. Once we account for electrode polarization effects, we are able to obtain quantitative mobilities in the low-frequency regime from our ac microelectrophoresis measurements; for these measurements, we use poly(methyl methacrylate) colloids that are gravitationally confined to a plane while suspended in a low-polar solvent mixture of cis-trans decahydronaphthalene and CHB. We find that the dimensionless electrophoretic mobility is constant, consistent with expectations for frequencies below the ion-diffusion frequency, and has a value $E = 1.6 \pm 0.4$.



INTRODUCTION

Colloids in partially polar suspensions have proved to be a very valuable model system for tunable control of colloidal crystal phases.^{1–3} These partially polar suspensions are academically important: an experimental colloidal model system where density and refractive index of solvent and particle can be simultaneously matched, poly(methyl methacrylate) (PMMA) colloids in a mixture of a partially polar solvent (bromocyclohexane) and an apolar solvent (decahydronaphthalene), has been used to realize numerous crystalline phases and has also been used in studies of glassy behavior.^{4–6} Structure formation due to electrostatic effects is important in opposite-charged colloids constructed both from partially polar, nonaqueous systems as well as highly polar, aqueous systems.^{3,7} Electrostatic effects in partially polar solvents (for the purpose of this work we identify this as a solvent mixture with dielectric constant between 3 and 10) have also had industrial importance for decades;⁸ nevertheless, the frequency-dependent charging in such solvents has been inadequately characterized.

One aspect to tunability in this system that relates directly to the partially polar nature of the solvent is the rich phase behavior exhibited in the presence of external electric fields. Numerous experiments have been carried out in the high-frequency (megahertz) regime where the colloids behave as effective dipoles, resulting in new colloidal crystal phases,¹ phase transformations,⁹ and cluster structures.¹⁰ There have also been interesting nonequilibrium effects, band and lane formation, observed in the low-frequency regime where ionic transport (electrokinetic) effects are likely also to be very important.¹¹ Despite many in-depth studies examining colloidal phase behavior using this system, electrokinetics in low-polar colloidal suspensions has only been partially addressed.^{12–14}

Most colloid microscopy experiments are carried out in refractive-index matched solvents to enable visualization deep inside the sample. In systems that are refractive-index matched, light scattering-based electrophoresis measurements are more challenging, and microelectrophoresis utilizes direct microscopic observation of colloidal motion in the presence of electric fields in microfluidic cells.¹³ The alternating current (ac) electrophoresis is a useful method to obtain particle charge while eliminating or quantitatively accounting for electrode polarization effects (an example of its use is in the measurement of the charge of red blood cells¹⁵).

In this work, we report impedance spectroscopy and microelectrophoresis measurements of PMMA colloids in a solvent mixture that contains bromocyclohexane (CHB), which has a dielectric constant $\epsilon_s = 7.9$; this makes the solvent mixture partially polar. From these measurements, we can extract electrophoretic mobilities in ac fields with a frequency between 0.25 and 10 Hz. In this frequency range, our impedance spectroscopy measurements indicate that electrode polarization is quantitatively important. We then employ corrections due to electrode polarization to correct the measured mobilities.

METHODS

Impedance Spectroscopy. Cells for impedance spectroscopy were made with ITO-coated transparent and conducting ($20\text{--}30 \Omega$) glass plates. Some of the coated area was removed using HCl solvent, in order that the voltage is applied only in the area where the solvent is filled.

Received: March 10, 2017

Revised: April 21, 2017

Published: April 25, 2017

A potentiostat/galvanostat (Princeton Applied Research model 273A) attached to a lock-in amplifier (Signal Recovery model 5210) was used as the impedance spectrometer. The electrolyte capacitance that was measured by the impedance spectrum was tested and corrected for stray capacitance C^{stray} by measuring the empty cell capacitance C_{meas} prior to filling, and also obtaining a calculated value C_{calc} by carefully measuring the active area and the sample thickness using an optical microscope. The measured capacitance was larger than the calculated capacitance, likely arising from stray capacitance from the cabling, that is, in parallel to the sample capacitance. We thus obtained $C^{\text{stray}} = C_{\text{meas}} - C_{\text{calc}}$ and used this to correct the measured capacitance. We cross-checked our calibrations against two solvents with reliable literature values for dielectric constants in the range of interest: bromocyclohexane, $\epsilon_{\text{CHB,meas}} = 7.97 \pm 0.08$, $\epsilon_{\text{CHB,lit}} = 7.92$ and dodecane, $\epsilon_{\text{dodecane,meas}} = 1.98 \pm 0.01$, $\epsilon_{\text{dodecane,lit}} = 1.99$.

ac Microelectrophoresis and Self-Diffusion. For the ac microelectrophoresis and self-diffusion experiments, cells were made using a microscope slide as a base, on to which a series of machine cut stainless steel shims were bonded. These shims were used as the electrodes. On top of the metal shims a glass cover slide was added as a cover (thickness ~ 0.15 mm). The entire setup was bonded together using an ultraviolet-curing glue and was clamped for flatness. After this, wires were attached to the stainless steel shim electrodes, the cell was filled using capillary action, sealed, and used as soon as possible. In this geometry, the X - Y plane was imaged, and the shims were aligned with respect to the camera such that the field was along the X -direction. The electrode spacing is 1 mm, and the displacements are measured in the middle $200 \mu\text{m}$, that is, at least 0.4 mm from either shim.

The output of a function generator (Tektronix AFG3002) was attached to both an oscilloscope (Tektronix TDS1002) and a wideband amplifier (Krohn-Hite Corporation model 7662M) and then connected to the sample cell. The signal was back fed into the oscilloscope using a divide-by-10 oscilloscope probe (Tektronix P2220) such that the output peak to peak voltage could be read.

Finally the sample cell was placed within an upright optical microscope (Nikon Eclipse 80i) with a camera attached. For the first set of experiments (EH01), the Qimaging QICAM fast1394 camera (model QIC-F-CLR-12-C) was used, whereas an sCMOS PCO.Edge 5.5 camera was used for the second set (EH02). The frame rate for EH01 was 2.4 fps (0.416 s per frame), while the frame rate for EH02 was 30 fps (0.033 s per frame), allowing data acquisition at the higher frequencies. In both cases fluorescence microscopy was used to track the particles due to its enhanced rejection of nonfluorescing objects and its rejection of scattered incident light.

Experiments were done using $1 \mu\text{m}$ radius, fluorescent-labeled (NBD dye, blue excitation) PMMA colloidal particles (purchased from Andrew Schofield, the University of Edinburgh) at area fractions of around 0.08. Particle centroids are obtained using image processing carried out in the IDL environment using standard particle tracking techniques.¹⁶ The same software¹⁷ was also used to calculate mean-squared displacements. The average number of unique particles that were tracked for more than 60 frames was 350.

In three dimensions, the electrophoretic mobility is expected to exhibit a weak concentration dependence $\mu = \mu_0 (1 - C\Phi)$, where C is a constant that is close to unity.^{18,19} As will be seen this is smaller than the uncertainties in the current work.

The apolar solvents (cis-trans decahydronaphthalene or dodecane) were used as received. CHB solvent was filtered through a column of activated alumina and glass wool using a scaled-up version of a previous described procedure¹² with the goal being to consistently remove protic contaminants such as HBr and water.

RESULTS

Analysis of Particle Motions. An example of an experiment shown in Figure 1 ($f = 500\text{mHz}$, $E_0 = 7 \text{ V/mm}$) shows particles undergoing diffusive (along X and Y) and driven motion (along X) simultaneously. In the absence of an external field

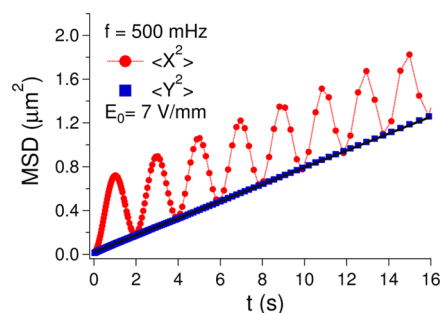


Figure 1. MSD along X and Y . There is linear behavior of the MSD as a function of time t along Y , characteristic of self-diffusion, and a sum of linear and oscillatory behaviors along X . $f = 500 \text{ mHz}$, $E_0 = 7 \text{ V/mm}$. The field is along X , and the image plane is the X - Y plane.

$$\langle Y^2(t) \rangle = \langle X^2(t) \rangle = 2Dt \quad (1)$$

For a given time t , we obtain $\langle X^2(t) \rangle$ and $\langle Y^2(t) \rangle$ where $\langle \rangle$ is a sum over particles as well as over the reference start time (in terms of the real time $t' = t + t_{\text{ref}}$).

With position given by a sinusoidal oscillation in addition to the diffusive contribution, the displacement is $X(t) = A[\sin \omega(t + t_{\text{ref}}) - \sin \omega t_{\text{ref}}] + \xi$ where $\omega = 2\pi f$ is the angular frequency of the electrophoretic driving and ξ is the random Brownian contribution. After integrating over reference start times t_{ref} one obtains the mean-squared displacement (MSD)

$$\langle X^2 \rangle = 2Dt + 2A^2 \left(\sin \left(\frac{\omega t}{2} \right) \right)^2 \quad (2)$$

In the direction perpendicular to the driving

$$\langle Y^2 \rangle = 2Dt \quad (3)$$

Assuming no coupling between diffusion and driven motion (this assumption can break down at high driving), the difference

$$\begin{aligned} X_{\text{driv}}^2 &\equiv \langle X^2 \rangle - \langle Y^2 \rangle \\ &= 2A^2 \left(\sin \left(\frac{\omega t}{2} \right) \right)^2 \\ &= A^2 (1 - \cos(\omega t)) \end{aligned} \quad (4)$$

yields the electrophoretic contribution to the motion. As can be seen in Figure 1, the mean-squared displacement (MSD) along X appears to be a sum of sinusoidal oscillatory term and a linear diffusive term that is identical to the MSD along Y . The above is useful: unlike an analysis of the displacement directly, this ac analysis allows us to be rid of the diffusive contribution. The averaging over reference start times t_{ref} yields a time dependence with a frequency $f = \omega/2\pi$, not $2f$.

We consider in Figure 2 an example of ac microelectrophoresis at $f = 250 \text{ mHz}$ and applied electric field amplitudes ranging from 7 to 60 V/mm. At both low and high amplitudes, there is no dependence of the MSD along Y on the driving field (which is along X). The MSD along the direction of the driving field (X) is identical, once per cycle (i.e., stroboscopically), to the MSD along Y , and exhibits a $\sin^2(\omega t/2)$ oscillation superimposed on the linear, diffusive time dependence.

Figure 2a shows a plot of $X_{\text{driv}}^2 = \langle X^2 \rangle - \langle Y^2 \rangle$ (shown on a log scale) as a function of time. The frequency dependence is sinusoidal and the time dependence with a frequency f (not $2f$)

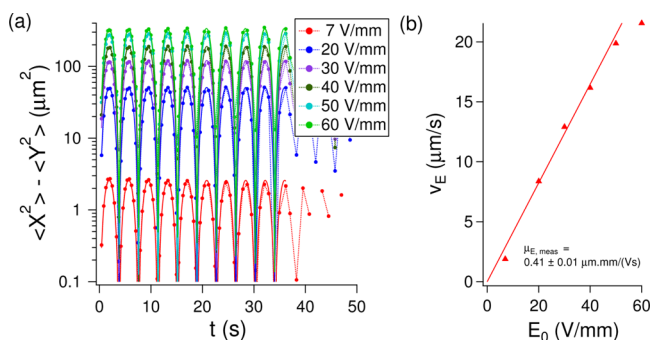


Figure 2. Amplitude dependence of ac microelectrophoresis. (a) The difference in the mean-squared displacement ($\langle X^2 \rangle$) along the direction of the driving field and the MSD along Y is $\langle X^2 \rangle - \langle Y^2 \rangle$, and it exhibits a pure $\sin^2(\omega t/2)$ oscillation with an amplitude A that increases with applied field E_0 at a frequency $f = \omega/(2\pi)$. For the plot shown, $f = 250$ mHz. (b) From the amplitude A , we obtain the particle velocity amplitude v_E as a function of E_0 .

is indeed observed. From a fit to eq 4, we obtained the amplitude A of the sinusoidal displacement. The velocity amplitude $v_E = 2\pi f A$. The electrophoretic mobility is obtained from the ratio of observed velocity and the internal electric field

$$v_E = \mu_E E_{\text{int}} \quad (5)$$

We denote the measured mobility $\mu_{E, \text{meas}} = v_E/E_0$, where E_0 is the applied electric field. From the dependence of v_E on the field amplitude E_0 , we get $\mu_{E, \text{meas}}$ from a linear fit in Figure 2b.

A second example (Figure 3) shows the frequency dependence at a fixed external field amplitude. No fits are

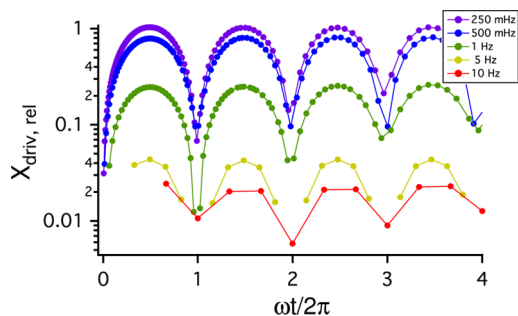


Figure 3. Frequency dependence of ac microelectrophoresis: Scaled $X_{\text{driv, rel}} = \sqrt{\langle X^2 \rangle - \langle Y^2 \rangle}$ plotted versus $\omega t/2\pi$ at the lowest field amplitude. At higher frequencies the amplitude of oscillation decreases, and higher field amplitudes are required to obtain reliable fits to the oscillation. Before one obtains the frequency dependence quantitatively, one needs to address electrode polarization corrections. $E_0 = 7$ V/mm.

shown here; it is clear that at the highest frequency (10 Hz) one needs larger driving field amplitudes in order to obtain reliable fits to the sinusoidal behavior of eq 4.

Two corrections are first necessary. First, in order to know this internal field, we need a quantitative measure of the electrode polarization contribution. Second, the velocity must be corrected for substrate proximity effect (the so-called Faxén law²⁰); that is, the hydrodynamic slowing down of spherical colloids close to a flat wall. We can correct, experimentally, using the diffusion coefficient D_Y (obtained from $\langle Y^2 \rangle$) and the bulk diffusion coefficient D_0 . Additionally, D_Y is noted to be close to the values for diffusion coefficient obtained in either X

or Y direction in the same sample once the field is turned off. These two corrections are addressed in the following two sections.

From these two corrections, we get the particle electrophoretic mobility

$$\mu_E = \mu_{E, \text{meas}} \left[\frac{E_0}{E_{\text{int}}} \right] \left[\frac{D_0}{D_Y} \right] = \mu_{E, \text{meas}} \cdot \gamma_E^{-1} \delta^{-1} \quad (6)$$

where $\gamma_E = E_{\text{int}}/E_0$ is the (sizable) attenuation factor due to electrode polarization and $\delta = D_Y/D_0$ is the correction factor due to electrode proximity. The former correction (γ_E) is a more complicated correction. The latter (δ) is a straightforward correction and is discussed next.

Velocity Profiles and Substrate Proximity Effects. In normal bulk electrophoresis, one can either have a parabolic flow profile or a plug flow velocity profile in the Z -direction, that is, perpendicular to the direction of particle motions. In our system, however, all the particles are within a few micrometers of the top surface and with a field along X one expects a flow profile that is akin to electro-osmosis (indeed the only distinction from electro-osmosis is the size of the ion). Any back flow due to the particle motions, should happen in the bulk of the cell, and given the small number of particles near the top and the large particle-free volume below them, the back flow is expected to be small.

In principle, the observed particle motion could arise from the particles responding to the electric field directly, from fluid flow induced by electro-osmosis, or from both. In fact, one can measure electro-osmosis independently by measuring dye motion in a field.²¹ In the present experiments, we discount electro-osmosis for the following reason. While the experiments are carried with all the particles sedimented to the top substrate, the sample when initially prepared is more uniformly distributed through the cell, although there are far fewer particles in the bottom half of the sample cell by the time the experiment is begun. When an electric field is applied in this transient state, we see uniform (back-and-forth) particle motions for all particles in the cell, without no noticeable flows in the reverse direction anywhere in the cell.

Even when the particle motion is electrophoretic, the particle mobility $\mu_{\text{eff}} \equiv D/k_B T$ is nevertheless affected by proximity to the surface, due to hydrodynamic interactions with the flat wall. Thus, for each field we need to estimate the correction to the effective viscosity. We obtain the effective viscosity from the measured diffusion coefficient in the direction perpendicular to the field. Specifically, for a colloidal particle drifting steadily in a medium of viscosity η in a force F , $v_0 = \mu_0 F$ where μ_0 is the bulk particle mobility. Close to the surface, the measured drift speed $v = \mu_{\text{eff}} F$, where μ_{eff} is the same mobility as in the observed diffusion coefficient in the absence of an external force. Thus,

$$v = v_0 \frac{\mu_0}{\mu_{\text{eff}}} = v_0 \frac{D_0}{D}$$

For each experiment, we obtain the self-diffusion in the Y direction ($\langle Y^2 \rangle$ is seen to always be linear in time) as well as the $\langle X^2 \rangle$ which gives us the microelectrophoretic information (Figure 1). The ratio D_0/D_Y is obtained as the experimentally determined hydrodynamic correction factor of the colloid mobility due to electrode proximity for each experiment, where D_0 is the bulk self-diffusion coefficient of the colloids in the bulk (measured separately).

Electrode Polarization in Low-Polarity Solvents. Following Schwan,²² we may write a phenomenological form

for the parallel combination of the measured components R and C of the impedance Z (i.e., $1/Z = 1/R + j\omega C$) as a function of $\omega = 2\pi f$, including the effect of electrode polarization, assuming that the electrode polarization components (C_p , R_p) are in series with each other and with the parallel combination of the sample impedance components (C_s , R_s)

$$R = [1 + (R\omega C)^2] \left[R_p + \frac{R_s}{1 + (R_s\omega C_s)^2} \right] \quad (7)$$

and

$$\frac{1}{\omega C} = \left[1 + \frac{1}{(R\omega C)^2} \right] \left[\frac{1}{\omega C_p} + \frac{\frac{1}{\omega C_s}}{1 + \left(\frac{1}{R_s\omega C_s} \right)^2} \right] \quad (8)$$

Furthermore, C_p and R_p are typically not constant but have the phenomenological power law form $C_p = C_{p0}f^{-m}$ and $R_p = R_{p0}f^{-n}$.

The measured resistance and capacitance for pure CHB solvent (and electrode spacing $d = 276 \mu\text{m}$) are shown in Figure 4. The resistance values were seen to be noisy above 10^4

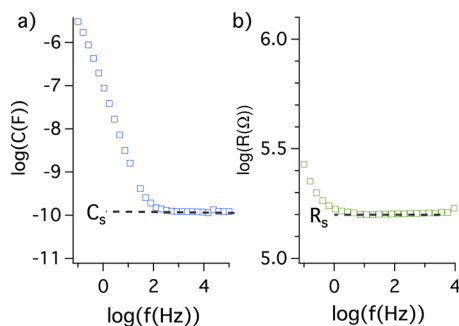


Figure 4. Electrode polarization effects. The measured (a) capacitance C and (b) resistance R as a function of frequency for CHB solvent with cell thickness $d = 276 \mu\text{m}$, reach a plateau at the solvent values C_s and R_s at high frequencies. At low frequencies, the measured capacitance increases by several orders of magnitude, while the measured resistance shows a less dramatic increase by about 50%.

Ω , and thus all fitting is carried out only to frequencies lower than this upper cut off. At low frequencies (below 100 Hz), the

capacitance is seen to change by more than 5 orders of magnitude. The measured resistance on the other hand, has a much more modest frequency dependence below 1 Hz.

At low frequencies, the right-hand side of eq 8 is dominated by the C_p term (i.e., the polarization capacitance), while at high frequencies the capacitance decreases to the value of C_s (the solvent capacitance); this behavior is seen in Figure 4a, where we can directly extract the solvent capacitance from the high-frequency plateau: $C_s = 1.21 \pm 0.05 \times 10^{-10}$ F.

From eqs 7 and 8 we can write a more convenient form that involves only the measured (dimensionless) “time constant”

$$\omega\tau_{\text{exp}} = \omega RC = \frac{\frac{1}{\omega C_p} + \frac{1/\omega C_s}{1 + (1/R_s\omega C_s)^2}}{R_p + \frac{R_s}{1 + (R_s\omega C_s)^2}} \quad (9)$$

which represents all the measured quantities on the left-hand side of the equation. The low-frequency dependence of ωRC is $\sim 1/(\omega f^{-m}) \sim f^{-1+m}$, while the high-frequency dependence is dominated by the solvent impedance and should scale as f^1 .

Figure 5a shows the measured $\log(\omega RC)$ as a function of the frequency f (on a log scale). The low-frequency behavior scales as $f^{-0.75}$, consistent with $m = 0.25 \pm 0.02$. The high-frequency behavior scales as f^1 with a clear crossover frequency f_c identifiable via the minimum between the low and high frequency regimes. Given that $\tau_{\text{exp}} = RC$ is dominated at low frequency by the increase in C , we can fit the data in Figure 5 very well to eq 9 by setting $R_p = 0$ and holding C_s to the plateau value. For completeness, we use the fitted ωRC to plot in Figure 5b $R/(1 + (\omega RC)^2)$ versus frequency. Holding the values of R_s and C_s , we can now fit for the polarization resistance $R_p = R_{p0}f^{-n}$. Self-consistently, we find $R_{p0} \sim 7.9(6) \times 10^3 \Omega$, that is, much less than $R_s (= 1.6(2) \times 10^5 \Omega)$.

From the solvent capacitance C_s , the dielectric constant $\epsilon_s = C_s/G$ may be obtained. In the above, $G = A/d = 1.73 \text{ m}$ is the cell constant for the measurement. In Figure 6, ϵ_s was measured in solvent mixtures of the partially polar CHB with an apolar solvent (decalin or dodecane) as a function of the weight fraction w of apolar solvent. The ϵ_s can be fit to a phenomenological polynomial form $8.0(1) - 10.1(5)w + 4.1(3)w^2$. It is worth noting that this dielectric constant can be varied continuously with w regardless of the specifics of the apolar solvent employed.

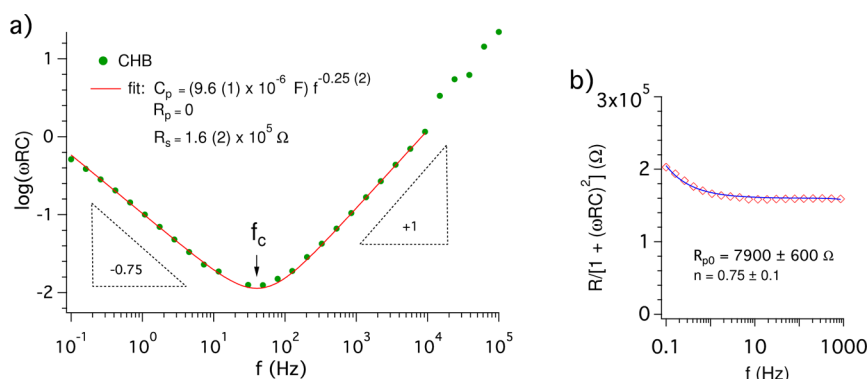


Figure 5. The measured time constant. (a) The measured ωRC as a function of frequency of CHB solvent (cell thickness $d = 276 \mu\text{m}$). (a) Fit of $\log(\omega RC)$ as a function of frequency to eq 9 yields R_s and $C_p = C_{p0}f^{-m}$ with fitted values indicated in the graph. R_p was set to zero. The minimum of the curve is the characteristic frequency f_c below which electrode polarization effects are relevant. (b) We can now fit $R/(1 + (\omega RC)^2)$ in eq 7 and obtain $R_p = R_{p0}f^{-n}$.

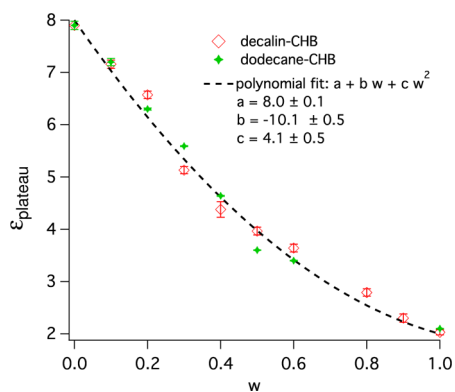


Figure 6. The dielectric constant ϵ_s . Obtained from the plateau C_s for binary solvent mixtures consisting of the low-polarity solvent CHB and a second solvent that is apolar—cis—trans decahydronaphthalene (decalin) or dodecane, ϵ_s is plotted as a function of the weight fraction w of decalin (or dodecane).

We also plot in Figure 7 the time constant plots for different w and for both decalin-CHB (Figure 7a) and dodecane-CHB

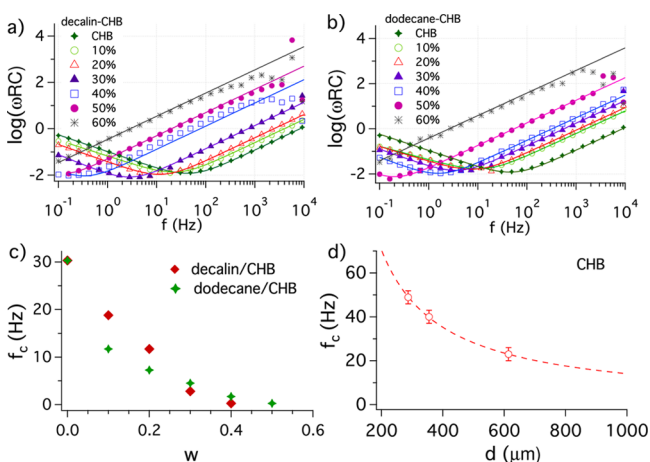


Figure 7. Dependence on solvent polarity. (a) $\log(\omega RC)$ versus f plotted for binary solvent mixtures consisting of the low-polarity solvent CHB and a second solvent that is apolar: (a) cis—trans decahydronaphthalene (decalin) and (b) dodecane. (c) A clear shift to lower frequencies, as a function of increasing apolarity, is seen in f_c (the crossover frequency which marks the low-frequency regime where electrode polarization dominates the measured time constant). The power law for the polarization capacitance across all these data sets is consistent with $m = 0.25 \pm 0.04$. (d) The dependence of f_c on sample thickness d (shown for pure CHB), is well described by a $1/d$ dependence (dashed line) expected for electrode polarization.

(Figure 7b). Good fits are obtained to the generic form of eq 9 for all w in both cases. A clear shift is seen in the cutoff frequency f_c , (Figure 7(c)) which exhibits a steady decrease from 30 Hz for pure CHB, and decreases to a value less than $f_c \sim 10$ Hz for $w \sim 0.2$, 5 Hz for $w \sim 0.3$, and 1 Hz for $w \sim 0.5$. Thus, for typical solvent mixtures that are chosen to match the density and/or refractive index of colloidal PMMA particles, electrode polarization are quantitatively important for frequencies less than 10 Hz. Note that this is orders of magnitude lower than the corresponding frequency regime for aqueous suspensions.²³ This is, however, the frequency regime for our microelectrophoresis experiments and electrode polarization corrections to the field are warranted.

Another test for electrode polarization is the expected inverse dependence on electrode spacing. In Figure 7d, we plot f_c obtained in pure CHB for three samples with different electrode spacings. The change in f_c is consistent with the expected $1/d$ dependence.

For completeness, we plot the electrical conductivity σ as a function of w in Figure 8a. Also plotted is the calculated

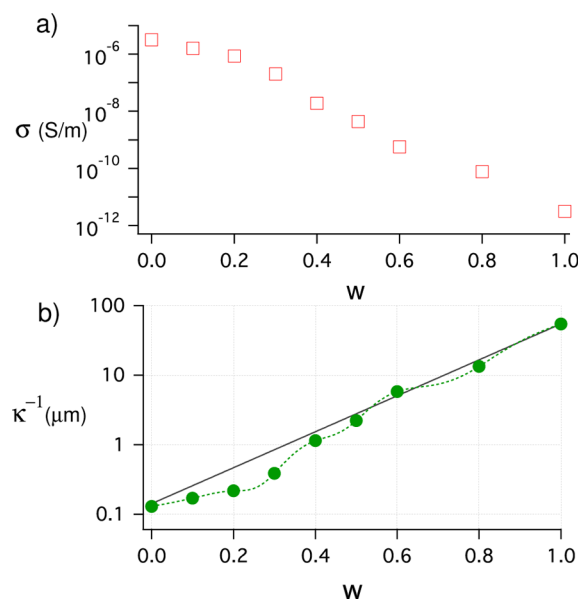


Figure 8. Conductivity, molar concentration, and Debye length for decalin-CHB. (a) Conductivity σ and molar concentration C_i as a function of w . (b) The Debye length κ^{-1} versus w .

quantity, the Debye length κ^{-1} (Figure 8(b)). C_i is obtained, as elsewhere,¹ using the relation $C_i[\text{mol/L}] = \sigma[\text{S/m}] \times \frac{1}{10^3 \Lambda^m} [\text{mol/S}\cdot\text{m}^2]$ and obtaining Λ^m using Walden's rule ($\Lambda^m \eta^m = \Lambda^w \eta^w$). In the above, m refers to the mixture and w refers to water, and Λ^w and η^w for water is $146 \text{ S}\cdot\text{cm}^2/\text{mol}$ and $0.894 \text{ mPa}\cdot\text{s}$ respectively,²⁴ while η^m was measured to be $2.1 \text{ mPa}\cdot\text{s}$. The Debye screening lengths, κ^{-1} , can then be determined, $\kappa^{-1} = (0.344 \times 10^{-10} \text{ m}) \sqrt{\frac{\epsilon_s}{C_i}}$. An exponential fit in Figure 8b is shown as a guide to the eye; the real behavior appears to deviate systematically from this functional form.

Colloidal Dynamics in ac Electric Fields. The ac microelectrophoresis experiments were carried out for frequencies ranging from 0.25 to 100 Hz. We may calculate the internal electric fields E_{int} from the applied electric field E_0 ; $E_{\text{int}} = \gamma_E E_0$ where the attenuation factor (following Kang et al.²⁵)

$$\gamma_E = \Omega / \sqrt{4 + \Omega^2} \quad (10)$$

In eq 10, $\Omega = \omega L / D\kappa$, where Ω is a dimensionless frequency constructed from $\omega = 2\pi f$, the electrode spacing is L , the ion diffusion coefficient is D , and κ is the inverse of the solvent Debye length which was obtained from the conductivity measurements (reported in Figure 8). One can alternately write $\Omega = f/f_c^{\text{model}}$, where $f_c^{\text{model}} = D/(2\pi L\kappa^{-1})$ is a characteristic frequency below which attenuation corrections are important. A comparison of f_c^{model} with f_c for CHB is shown in Figure 9; it is apparent that while the behavior is qualitatively similar with a

sharp decrease of f_c with w , there are quantitative differences at larger w .

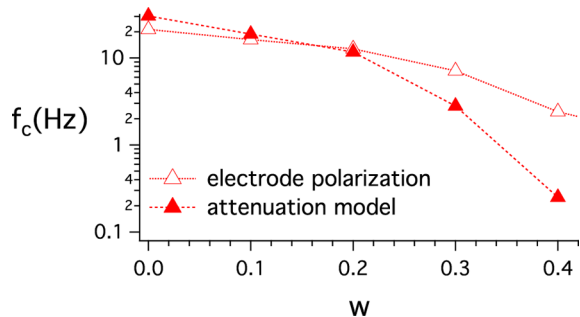


Figure 9. Characteristic frequencies. A comparison between measured f_c (decalin–CHB) with those from an attenuation model $f_c^{\text{model}} = D/(2\pi L\kappa^{-1})$ shows some deviations at larger w .

For the system in microelectrophoresis (32.5% decalin by volume, corresponding to $w \approx 0.24$), $\kappa^{-1} \approx 0.3 \mu\text{m}$. Using an ion diffusion coefficient of $D = 0.48 \times 10^{-9} \text{ m}^2/\text{s}$ (scaling the bromide ion diffusion coefficient in water of $1.18 \times 10^{-9} \text{ m}^2/\text{s}$ ²⁶ by the ratio of measured viscosities in water, 0.89 mPa·s, and the decalin–CHB mixture, 2.1 mPa·s, at 25 °C), and electrode spacing $L = 1 \text{ mm}$, we can then obtain the attenuation factor γ as a function of frequency; this is shown in Figure 10 (solid red

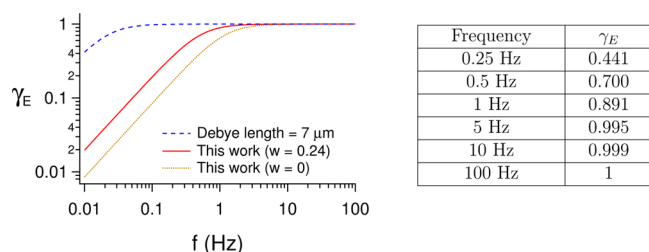


Figure 10. Attenuation factor γ_E as a function of frequency for a 32.5:67.5 (v/v) decalin–CHB solvent mixture ($w = 0.24$) using Debye lengths from Figure 8b in this work; below 5 Hz, there is significant reduction in the internal electric field due to electrode polarization. Also shown for comparison are the attenuation factor expected for significantly larger Debye lengths ($\kappa^{-1} = 7 \mu\text{m}$) and for pure CHB (this work, $w = 0$). Tabulated are the values of γ_E for the frequencies used in the experiment ($w = 0.24$).

curve). Shown for comparison in Figure 10 are the attenuation factor expected for significantly larger Debye lengths (blue dashes, $\kappa^{-1} = 7 \mu\text{m}$) and for pure CHB (yellow dots, $w = 0$). Also tabulated in Figure 10 are the attenuation factors for the frequencies employed in the current work. In both, we see that there is significant reduction in the internal electric field due to electrode polarization below 5 Hz.

Next, we plot (Figure 11) μ_E as a function of frequency in the range 250 mHz to 10 Hz. Each data point in this graph comes from a series such as is shown in Figure 2. The closed and open symbols correspond to two separate runs (with cameras with different frame rates; details in Methods). As was seen in Figure 3, as one goes to higher frequency one needs better position- and time-resolution; this sets 10 Hz as the limit for our microelectrophoresis measurements. The experiments carried out at 100 Hz exhibit identical particle motions along X and Y and identical to those at zero field, indicating that there are no

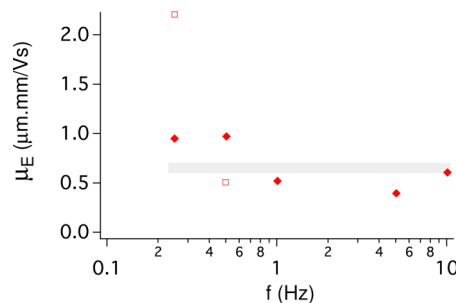


Figure 11. The ac electrophoretic mobility as a function of driving frequency after corrections for electrode polarization attenuation and substrate proximity. Open/filled symbols (EH01/EH02) refers to different samples with images acquired at 2.4 fps and 30 fps, respectively.

induced-charge electro-osmotic forces²⁷ because those effects remain active at nonzero frequencies.

The electrophoretic mobility μ_E is roughly constant, $\mu_E = 0.65 \pm 0.20 \mu\text{m}\cdot\text{mm}/\text{V}\cdot\text{s}$, in the frequency range between 500 mHz and 10 Hz. At 250 mHz, it is apparently significantly larger for one of the two samples (EH01) but not the other (EH02). This value is comparable with previous direct current (dc) measurements,^{12,13} which found $\mu_E \approx 0.4\text{--}0.5 \mu\text{m}\cdot\text{mm}/\text{V}\cdot\text{s}$ (without considering electrode polarization effects). The large scatter in the data does not come from intrinsic measurement errors, which comes from fits of the v_E versus E plots and is smaller than the symbols used. Instead, it comes from experiment-to-experiment variations, which are a known challenge for experimenters using these partially polar systems.

In principle, the electrophoretic mobility is frequency dependent,^{28,29} relating to the response time for the double layer. Simulations of the dependence of the electrophoretic mobility on the dimensionless frequency do predict a sharp decrease,²⁸ but the characteristic frequencies in the problem are the momentum diffusion frequency $f_M = \eta/(\rho a^2)$, and the ion diffusion frequency $f_D = D/(2a)^2$. Given $\eta = 2.1 \text{ mPa}\cdot\text{s}$, $\rho = 1.18 \times 10^3 \text{ kg}/\text{m}^3$, $D = 0.5 \times 10^{-9} \text{ m}^2/\text{s}$, and $a = 1 \times 10^{-6} \text{ m}$, the values for the characteristic frequencies in our system are $f_M \sim 1 \text{ MHz}$ and $f_D \sim 100 \text{ Hz}$. Therefore, for our experiments the frequency $f \ll f_D \ll f_M$, and in this regime the simulated mobilities are constant. Thus, we expect to be obtain the dc value from our measurements.

With $\epsilon_s = 5.9$ and $\eta = 0.0021 \text{ Pa}\cdot\text{s}$, one may use this electrophoretic mobility (along with the O'Brien and White scheme³⁰) to obtain a dimensionless mobility $E = \frac{3\eta e}{2\epsilon_s \epsilon_0 k_B T} \mu_E = 1.6 \pm 0.4$, and a dimensionless Zeta potential, $\Psi = 1.5 \pm 0.4$ ($\zeta = \Psi k_B T/e \sim 37 \text{ mV}$). This, along with $\kappa a \sim 3.3$, can be further converted into a particle charge Z using the empirical relation following Leunissen,¹² (also, see Hunter³¹)

$$Z = 4\pi\epsilon_s\epsilon_0 \frac{k_B T}{e} \kappa a^2 \left[2 \sinh\left(\frac{\Psi}{2}\right) + \frac{4}{\kappa a} \tanh\left(\frac{\Psi}{4}\right) \right] \quad (11)$$

For our work, we obtain $Z = 720 \pm 180e$.

CONCLUSION

Partially polar colloidal systems are very valuable for microscopy studies of crystallization and the glass transition because both density and refractive index of particle can be matched with that of the solvent, and because the interparticle

interactions are tunable.^{1,3,4} In this work, we show that microelectrophoresis can be extended to ac measurements conveniently in these partially polar colloidal systems. Because of the strong variation of the polarity with weight fraction of the apolar solvent (Figure 6), measurements need to be done at the precise solvent mixture used in microscopy experiments: yet this is the concentration where scattering is minimized by refractive index matching and traditional electrophoresis measurements are thus harder. We discuss a simple scheme to obtain the driven (electrophoretic) contribution for small driving where the response is linear and in the presence of self-diffusion. More precise measurements can undoubtedly be made in a cell where corrections for substrate proximity are not necessary but we note that the current scheme can be realized in situ in the context of a confocal microscopy experiment in a colloidal system.

Obtaining quantitative estimates of the electrophoretic mobility requires a systematic accounting of electrode polarization effects, which we present. Such electrode polarization analyses (Figures 3–6) establish first that electrode polarization is clearly quantitatively important below a characteristic frequency f_c that increases with increasing polarity of the solvent and decreases inversely with sample thickness. Consideration of such effects is necessary in order to obtain reliable mobilities and is definitely relevant in microscopy experiments where the electrode spacing is often the sample thickness (i.e., $d < 200 \mu\text{m}$). The electrode polarization capacitance is seen, as a function of the frequency f , to obey a very clear power law behavior, $C_p = C_0 f^{-m}$, with $m = 0.25 \pm 0.04$.

As noted elsewhere,¹⁴ dc measurements¹³ would be even more prone to such effects; in fact, the steady-state internal field with an applied dc field (with significant counterions in solution) should be zero, so the comparable values obtained in previous work could arise from being measured in the transient. It is also true that the previous measurements, done at very large κ^{-1} , should have a weaker electrode polarization effect due to the lower ion concentrations: a rough estimate suggests that at $\kappa^{-1} \sim 7 \mu\text{m}$, electrode polarization effects should be quantitatively important only below 0.1 Hz (blue dashed curve in Figure 10). The current measurements are, however, likely reflective of real confocal microscopy experiments at higher colloid concentrations. For this system, it should be noted that all that was needed to obtain a quick estimate of the characteristic frequency f_c and the attenuation factor γ_E was a knowledge of sample and solvent parameters needed for eq 10.

Future work will include examination of the effects of chain formation observed at higher fields on microelectrophoretic dynamics. Furthermore, it is feasible at high fields that the assumption of no coupling between driven and diffusive motion (eq 4) will break down. Examining this breakdown will be the ongoing focus.

AUTHOR INFORMATION

Corresponding Author

*E-mail: ayethiraj@mun.ca

ORCID

Anand Yethiraj: 0000-0003-1293-2801

Notes

The authors declare no competing financial interest.

ACKNOWLEDGMENTS

This work was supported by the Natural Sciences and Engineering Research Council of Canada. We thank Kris Poduska for generously providing access to the impedance spectrometer hardware and software, and to Jiaqi Cheng for a tutorial on its use. Gordon Whelan is thanked for help with early versions of the dielectric cell. A.Y. acknowledges useful discussions with Jure Dobnikar, Andrew Hollingsworth, and Jan Dhont. E.H. and Z.A. contributed equally to this work.

REFERENCES

- (1) Yethiraj, A.; van Blaaderen, A. A colloidal model system with an interaction tunable from hard sphere to soft and dipolar. *Nature* **2003**, *421*, 513–517.
- (2) Yethiraj, A. Tunable colloids: control of colloidal phase transitions with tunable interactions. *Soft Matter* **2007**, *3*, 1099–1115.
- (3) Leunissen, M. E.; Christova, C. G.; Hynninen, A. P.; Royall, C. P.; Campbell, A. I.; Imhof, A.; Dijkstra, M.; van Roij, R.; van Blaaderen, A. Ionic colloidal crystals of oppositely charged particles. *Nature* **2005**, *437*, 235–240.
- (4) Stadner, A.; Sedgwick, H.; Cardinaux, F.; Poon, W.; Egelhaaf, S.; Schurtenberger, P. Equilibrium cluster formation in concentrated protein solutions and colloids. *Nature* **2004**, *432*, 492–495.
- (5) Capellmann, R. F.; Valadez-Pérez, N. E.; Simon, B.; Egelhaaf, S. U.; Laurati, M.; Castañeda-Priego, R. Structure of colloidal gels at intermediate concentrations: the role of competing interactions. *Soft Matter* **2016**, *12*, 9303–9313.
- (6) Sentjabrskaja, T.; Zaccarelli, E.; De Michele, C.; Sciortino, F.; Tartaglia, P.; Voigtmann, T.; Egelhaaf, S. U.; Laurati, M. Anomalous dynamics of intruders in a crowded environment of mobile obstacles. *Nat. Commun.* **2016**, *7*, 11133.
- (7) Russell, E. R.; Sprakel, J.; Kodger, T. E.; Weitz, D. A. Colloidal gelation of oppositely charged particles. *Soft Matter* **2012**, *8*, 8697.
- (8) Klinkenberg, A.; van der Minne, J. *Electrostatics in the Petroleum Industry. The Prevention of Explosion Hazards*; A Royal Dutch/Shell Research and Development Report; Amsterdam, 1958.
- (9) Yethiraj, A.; Wouterse, A.; Groh, B.; van Blaaderen, A. Nature of an Electric-Field-Induced Colloidal Martensitic Transition. *Phys. Rev. Lett.* **2004**, *92*, 058301.
- (10) Demirörs, A. F.; Stiefelhagen, J. C.; Vissers, T.; Smallenburg, F.; Dijkstra, M.; Imhof, A.; van Blaaderen, A. Long-Ranged Oppositely Charged Interactions for Designing New Types of Colloidal Clusters. *Phys. Rev. X* **2015**, *5*, 021012.
- (11) Vissers, T.; van Blaaderen, A.; Imhof, A. Band Formation in Mixtures of Oppositely Charged Colloids Driven by an ac Electric Field. *Phys. Rev. Lett.* **2011**, *106*. DOI: 10.1103/PhysRevLett.106.228303.
- (12) Leunissen, M. *Manipulating Colloids with Charges Electric Fields*. Ph.D. Thesis, Utrecht University, Amsterdam, The Netherlands, 2007.
- (13) Vissers, T.; Imhof, A.; Carrique, F.; Delgado, A. V.; van Blaaderen, A. Electrophoresis of concentrated colloidal dispersions in low-polar solvents. *J. Colloid Interface Sci.* **2011**, *361*, 443–455.
- (14) Lin, T.; Kodger, T. E.; Weitz, D. A. Transport of charged colloids in a nonpolar solvent. *Soft Matter* **2013**, *9*, 5173.
- (15) Chen, P. C. Y. Alternating current electrophoresis of human red blood cells. *Ann. Biomed. Eng.* **1980**, *8*, 253–269.
- (16) Crocker, J. C.; Grier, D. G. Methods of Digital Video Microscopy for Colloidal Studies. *J. Colloid Interface Sci.* **1996**, *179*, 298.
- (17) Crocker, J. C.; Weeks, E. R. *Particle tracking using IDL*; <http://www.physics.emory.edu/weeks/idl/>, 2008.
- (18) Anderson, J. L. Concentration dependence of electrophoretic mobility. *J. Colloid Interface Sci.* **1981**, *82*, 248–250.
- (19) Zukoski, C.; Saville, D. Electrokinetic properties of particles in concentrated suspensions. *J. Colloid Interface Sci.* **1987**, *115*, 422–436.

- (20) Happel, J.; Brenner, H. *Low Reynolds number hydrodynamics: with special applications to particulate media*; Springer Netherlands: Dordrecht, 1981.
- (21) Schwer, C.; Kenndler, E. Electrophoresis in fused-silica capillaries: the influence of organic solvents on the electroosmotic velocity and the zeta potential. *Anal. Chem.* **1991**, *63*, 1801–1807.
- (22) Schwan, H. P. Alternating current electrode polarization. *Radiat. Environ. Biophys.* **1966**, *3*, 181–201.
- (23) Beltramo, P. J.; Roa, R.; Carrique, F.; Furst, E. M. Dielectric spectroscopy of concentrated colloidal suspensions. *J. Colloid Interface Sci.* **2013**, *408*, 54–58.
- (24) Bockris, J. O. M.; Reddy, A. K. Modern electrochemistry, Volume 1: Ionics. *J. Chem. Educ.* **1999**, *76*, 1069.
- (25) Kang, K.; Dhont, J. K. G. Electric-field induced transitions in suspensions of charged colloidal rods. *Soft Matter* **2010**, *6*, 273–286.
- (26) Cussler, E. L. *Diffusion: mass transfer in fluid systems*, 2nd ed.; Cambridge University Press: New York, 1997.
- (27) Bazant, M. Z.; Squires, T. M. Induced-Charge Electrokinetic Phenomena: Theory and Microfluidic Applications. *Phys. Rev. Lett.* **2004**, *92*, 066101.
- (28) Shih, C.; Yamamoto, R. Dynamic electrophoresis of charged colloids in an oscillating electric field. *Phys. Rev. E* **2014**, *89*, 062317.
- (29) Zhou, J.; Schmid, F. Computer simulations of charged colloids in alternating electric fields. *Eur. Phys. J.: Spec. Top.* **2013**, *222*, 2911–2922.
- (30) Hunter, R. J. *Foundation of Colloid Science*; Oxford University Press, 2001.
- (31) Hunter, R. J.; Ottewill, R. H.; Rowell, R. L. *Zeta Potential in Colloid Science*; Elsevier, 1981.